http://dx.doi.org/10.5012/bkcs.2012.33.3.933

Behavior of Poisson Bracket Mapping Equation in Studying Excitation Energy Transfer Dynamics of Cryptophyte Phycocyanin 645 Complex†

Weon-Gyu Lee, Aaron Kelly,[a] and Young Min Rhee*

*Institute of Theoretical and Computational Chemistry, Department of Chemistry, Pohang University of Science and Technology (POSTECH), Pohang 790-784, Korea. *E-mail: ymrhee@postech.ac.kr*
Received December 5, 2011, Accepted January 7, 2012

Recently, it has been shown that quantum coherence appears in energy transfers of various photosynthetic light-harvesting complexes at from cryogenic to even room temperatures. Because the photosynthetic systems are inherently complex, these findings have subsequently interested many researchers in the field of both experiment and theory. From the theoretical part, simplified dynamics or semiclassical approaches have been widely used. In these approaches, the quantum-classical Liouville equation (QCLE) is the fundamental starting point. Toward the semiclassical scheme, approximations are needed to simplify the equations of motion of various degrees of freedom. Here, we have adopted the Poisson bracket mapping equation (PBME) as an approximate form of QCLE and applied it to find the time evolution of the excitation in a photosynthetic complex from marine algae. The benefit of using PBME is its similarity to conventional Hamiltonian dynamics. Through this, we confirmed the coherent population transfer behaviors in short time domain as previously reported with a more accurate but more time-consuming iterative linearized density matrix approach. However, we find that the site populations do not behave according to the Boltzmann law in the long time limit. We also test the effect of adding spurious high frequency vibrations to the spectral density of the bath, and find that their existence does not alter the dynamics to any significant extent as long as the associated reorganization energy is changed not too drastically. This suggests that adopting classical trajectory based ensembles in semiclassical simulations should not influence the coherence dynamics in any practical manner, even though the classical trajectories often yield spurious high frequency vibrational features in the spectral density.

Key Words : Semiclassical method, Quantum classical dynamics, Excited state, Excitation energy transfer, Photosynthesis

Introduction

Recently, there have been continued reports describing long-lived quantum coherence in energy transfer processes in pigment molecules of various photosynthetic light harvesting complexes. Experimentally, this coherence appears with quantum beating in populations of involved quantum states.[1-4] In a sense, this behavior is surprising because photosynthetic complexes are supposed to be in highly noisy environment where quantum dynamical characteristics may not last for a long time. Even though the coherence was first observed at cryogenic temperatures,[1,2] it was later found even at physiologically relevant temperatures with a marine cryptophyte algae system (Chroomonas CCMP270),[3] and later with Fenna-Matthews-Olson (FMO) complex.[4]

Of the two, the marine algae system is of particular interest partly because the experiment was performed really at room temperature (294 K) and the protein complex is from a more evolved species. Specifically, CCMP270 involves phycocyanin PC645 protein complex. In general, cryptophytes have tunable bilins, which render them to have different absorption features depending on the species. Additionally, they can photosynthesize even in low light conditions, evidencing that their energy transfer is very efficient.[5] PC645 possesses two dihydrobiliverdins (DBV), two mesobiliverdins (MBV), and four phycocynobilins (PCB) chromophores enfolded in four protein subunits.[6] Its structure was determined at 1.4 Å resolution by X-ray crystallography.[7] In the experiment,[3] the central DBV dimer was initially electronically excited with a laser pulse and the excitation energy was transferred to the MBV molecules. At the last stage, the four PCB molecules absorb the energy from the MBVs.[3]

When treating the system theoretically, as the pigment complex system is too large and too complicated to be treated by quantum mechanical approaches for all the variables, a quantum-classical method will be useful. One approach is the quantum-classical Liouville equation (QCLE): in this approach, the dynamics of excitations in the bilins will be treated with quantum degrees of freedom ("quantum subsystem") and their dynamics is usually described by its reduced density matrix. The remaining parts are treated as a "bath" that mostly follows classical mechanics. When the classical bath is composed of harmonic oscillators, it is known that the evolution of the density matrix with the bath is exactly

†This paper is to commemorate Professor Kook Joe Shin's honourable retirement.

[a]Present address: Department of Chemistry, Stanford University, Stanford CA 94305, United States.

governed by quantum-classical Liouville equation regardless of the number of bath modes.[8]

In this paper, we use an approximate version of QCLE, called Poisson bracket mapping equation (PBME). It was already presented with the FMO complex that PBME is reliable in predicting the coherent behaviors at reduced computational cost.[9] Here, we apply PBME formalism to study the exciton transfer dynamics in PC645 from Chroomonas CCMP270.[3] The model Hamiltonian we chose is the form adopted in a previous theoretical study by Huo and Coker with iterative linearized density matrix (ILDM) method for solving the quantum-classical equation.[10] In general, we find that PBME reproduces the more accurate but more time-consuming ILDM results very reliably. We then study the effect of changing the spectral density functions. The motivation for this investigation is the fact that the spectral densities from molecular dynamics (MD) simulation often show very different behaviors from simple model based densities (such as Debye or Ohmic types) and even from experimentally observed ones. The most prominent difference is the fact that the spectral densities from MD simulations have many large peaks in relatively high frequency regions (> ~1500 cm^{-1}). To investigate how such spurious peaks affect the coherence dynamics, we add artifactual Gaussian peaks to the original spectral density and then follow the changes in the excitation energy transfer dynamics. Finally, the long time behavior of PBME is investigated. Because PBME does not satisfy the fluctuation-dissipation theorem,[9,11] it is well expected that the long time behavior will deviate from the correct Boltzmann distribution. We indeed find such an artifact and observe that the population distribution is skewed toward the high temperature limit. Based on these findings, implications for future applications of PBME in realistic systems are also discussed.

Theory

Poisson Bracket Mapping Equation. The details of deriving the PBME equation have been already presented by earlier investigators.[12-15] Here, for completeness, we will give a brief overview. For solving the quantum-classical Liouville equation, we consider the partial Wigner transformation to the total system with respect to the variables of the environmental bath. Accordingly, the total Hamiltonian is transformed as

$$\hat{H}_W = \frac{P^2}{2M} + \frac{\hat{p}^2}{2m} + V_s(\hat{r}) + V_e(R) + V_c(R,\hat{r}) \tag{1}$$

Here, V_s, V_e, and V_c are respectively subsystem, bath, and subsystem-bath coupling potentials, and R and P denote N_e-dimensional coordinates and momenta of environmental degrees of freedom with mass M. Also, $\hat{r}$ and $\hat{p}$ are the operators for the phase space variables of the quantum subsystem with mass m. When we need to designate the position and momentum collectively, we will use X and x for the bath and the subsystem. We also define the subsystem Hamiltonian as

$$\hat{h}_s = \frac{\hat{p}^2}{2m} + V_s(\hat{r}) + V_c(R,\hat{r}) \tag{2}$$

with its eigenvalue ε_λ and eigenvector $|\lambda\rangle$ with a dimensionality N. The eigenvectors of course can form a subsystem basis.[8,12]

Now let us suppose a vector space consisting of eigenfunctions of N fictitious harmonic oscillators with only two allowed states with quantum numbers 0 and 1. We define a mapping basis within this space as $|m_\lambda\rangle = |0_1, 0_2, \cdots, 1_\lambda, \cdots, 0_N\rangle$ with the creation and annihilation operators $\hat{a}_\lambda^\dagger = (\hat{q} - i\hat{p})/\sqrt{2\hbar}$ and $\hat{a}_\lambda = (\hat{q} + i\hat{p})/\sqrt{2\hbar}$. Of course, the functional representation of the mapping basis can be formulated with the mapping basis coordinate q,

$$\begin{aligned}\langle q|m_\lambda\rangle &= \langle q_1, q_2, \cdots, q_\lambda, \cdots, q_N|0_1, 0_2, \cdots, 1_\lambda, \cdots, 0_N\rangle \\ &= \phi_0(q_1)\phi_0(q_2)\cdots\phi_1(q_\lambda)\cdots\phi_0(q_N)\end{aligned} \tag{3}$$

where the $\phi_v(q_\lambda)$ is the wavefunction of a harmonic oscillator with the quantum number v.

The subsystem basis can represent any subsystem operator $\hat{A}$ as $\Sigma_{\alpha\alpha'}^N A^{\alpha\alpha'}|\alpha\rangle\langle\alpha'|$ with $A^{\alpha\alpha'} = \langle\alpha|\hat{A}|\alpha'\rangle$. Also, it can be represented in the mapping space as $\hat{A} \to \hat{A}_m$, with a definition $\hat{A}_m = \Sigma_{\lambda\lambda'}^N A_m^{\lambda\lambda'} \hat{a}_\lambda^\dagger \hat{a}_{\lambda'}$. Thus,

$$A_m^{\lambda\lambda'} = \langle m_\lambda|A_m|m_{\lambda'}\rangle = \langle\lambda|\hat{A}|\lambda'\rangle \tag{4}$$

is symbolically satisfied. Also, let us denote the Wigner transforms of $\hat{H}_W$ and $\hat{h}_s$ as H_m and h_m, respectively, for future references. With the above information, one can show that the mapping Hamiltonian is

$$H_m = \frac{P^2}{2M} + V_e(R) + \frac{1}{2\hbar}\sum_{\lambda\lambda'} h_{\lambda\lambda'}(r_\lambda r_{\lambda'} + p_\lambda p_{\lambda'} - \hbar\delta_{\lambda\lambda'}) \tag{5}$$

with $h_{\lambda\lambda'}$ representing the matrix elements of the $\hat{h}_s$ operator.[8] The quantum-classical Liouville equation

$$\frac{d}{dt}\hat{O}_W(t) = \frac{i}{\hbar}[\hat{H}_W, \hat{O}_W(t)] - \frac{1}{2}(\{\hat{H}_W, \hat{O}_W(t)\} - \{\hat{O}_W(t), \hat{H}_W\}) \tag{6}$$

can also be represented with the mapping basis because all the operators in this equation are partial Wigner transformed and are defined in the subsystem space. By applying the mapping formulation to Eq. (6) with Eq. (4), followed by appropriate Wigner transformations, one can obtain

$$\begin{aligned}&\frac{d}{dt}O_m(x,X,t) \\ &= \frac{1}{\hbar}\sum_{\lambda\lambda'} h_{\lambda\lambda'}\left(p_\lambda\frac{\partial}{\partial r_{\lambda'}} - r_\lambda\frac{\partial}{\partial p_{\lambda'}}\right)O_m(t) + \left(\frac{P}{M}\frac{\partial}{\partial R} - \frac{\partial H_m}{\partial R}\frac{\partial}{\partial P}\right)O_m(t) \\ &\quad + \frac{\hbar}{8}\sum_{\lambda\lambda'}\frac{\partial h_{\lambda\lambda'}}{\partial R}\left(\frac{\partial}{\partial r_\lambda}\frac{\partial}{\partial r_{\lambda'}} - \frac{\partial}{\partial p_{\lambda'}}\frac{\partial}{\partial p_\lambda}\right)\frac{\partial}{\partial P}O_m(t)\end{aligned} \tag{7}$$

When the last summation is ignored,

$$\begin{aligned}\frac{d}{dt}O_m(x,X,t) &\approx \frac{1}{\hbar}\sum_{\lambda\lambda'} h_{\lambda\lambda'}\left(p_\lambda\frac{\partial}{\partial r_{\lambda'}} - r_\lambda\frac{\partial}{\partial p_{\lambda'}}\right)O_m(t) + \left(\frac{P}{M}\frac{\partial}{\partial R} - \frac{\partial H_m}{\partial R}\frac{\partial}{\partial P}\right)O_m(t) \\ &\equiv i\hat{L}O_m,\end{aligned} \tag{8}$$

where $-i\hat{L} = \{H_m, \bullet\}$. As the evolution of the operator O_m in the mapping basis is represented by this Poisson bracket, this evolution relationship is called the Poisson bracket mapping equation (PBME). By equating the total derivative in time (left hand side) together with the chain-rule formulations of (r, p, R, P), one can easily show that the mapping and bath coordinates and momenta behave exactly as in Hamilton's equations of motion:

$$\frac{dr_\lambda}{dt} = \frac{1}{\hbar}\sum_{\lambda'} h_{\lambda\lambda'}(R)p_{\lambda'},$$

$$\frac{dp_\lambda}{dt} = -\frac{1}{\hbar}\sum_{\lambda'} h_{\lambda\lambda'}(R)r_{\lambda'},$$

$$\frac{dR}{dt} = \frac{P}{M},$$

$$\frac{dP}{dt} = -\frac{\partial V_e}{\partial R} - \frac{1}{2\hbar}\left(r^T\frac{\partial h}{\partial R}r + p^T\frac{\partial h}{\partial R}p - \hbar\frac{\partial \mathrm{Tr}(h)}{\partial R}\right) \quad (9)$$

To find the time variation of the physical observable corresponding to $\hat{O}_W(t)$, we start from the mapping basis representation of its trace with the density matrix:

$$\langle O(t)\rangle = \sum_{\lambda\lambda'}\int\langle m_\lambda|\hat{O}_m(X,t)|m_{\lambda'}\rangle\langle m_{\lambda'}|\hat{\rho}_m|m_\lambda\rangle dX \quad (10)$$

For the first bracket in this equation, by applying the resolution of the identity in the coordinate space q and q',

$$\langle m_\lambda|\hat{O}_m|m_{\lambda'}\rangle = \int\langle m_\lambda|q\rangle\langle q|\hat{O}_m|q'\rangle\langle q'|m_{\lambda'}\rangle dq dq' \quad (11)$$

Substituting $q = r - z/2$ and $q' = r + z/2$, this equation becomes

$$\langle m_\lambda|\hat{O}_m|m_{\lambda'}\rangle = \int\langle m_\lambda|r-\frac{z}{2}\rangle\langle r-\frac{z}{2}|\hat{O}_m(X,t)|r+\frac{z}{2}\rangle\langle r+\frac{z}{2}|m_{\lambda'}\rangle dr dz \quad (12)$$

Applying the inverse Wigner transformation

$$\langle r-\frac{z}{2}|\hat{O}_m(X,t)|r+\frac{z}{2}\rangle = \frac{1}{(2\pi\hbar)^N}\int e^{-ipz/\hbar}O_m(x,X,t)dp, \quad (13)$$

Eq. (12) can be further modified as:

$$\langle m_\lambda|\hat{O}_m|m_{\lambda'}\rangle = \frac{1}{(2\pi\hbar)^N}\int g_{\lambda\lambda'}(x)O_m(x,X,t)dx, \quad (14)$$

where $g_{\lambda\lambda'}(x)$ is defined as

$$g_{\lambda\lambda'}(x) = \int\langle m_\lambda|r-\frac{z}{2}\rangle\langle r+\frac{z}{2}|m_{\lambda'}\rangle e^{-ipz/\hbar}dz \quad (15)$$

This quantity can be obtained analytically based on the coordinate representation of the mapping basis function, Eq. (3):

$$g_{\lambda\lambda'}(x) = \int\left[\phi_0\left(r_1-\frac{z_1}{2}\right)\cdots\phi_1\left(r_\lambda-\frac{z_\lambda}{2}\right)\cdots\phi_0\left(r_N-\frac{z_N}{2}\right)\right]^* \times\left[\phi_0\left(r_1+\frac{z_1}{2}\right)\cdots\phi_1\left(r_\lambda+\frac{z_\lambda}{2}\right)\cdots\phi_0\left(r_N+\frac{z_N}{2}\right)\right]e^{-i(p_1z_1+\cdots+p_Nz_N)/\hbar}dz \quad (16)$$

From the following three relationships,

$$\int\phi_0\left(r-\frac{z}{2}\right)\phi_0\left(r+\frac{z}{2}\right)e^{-ipz/\hbar}dz = 2e^{-\frac{r^2}{\hbar}}e^{-\frac{p^2}{\hbar}}, \quad (17)$$

$$\int\phi_1\left(r\mp\frac{z}{2}\right)\phi_0\left(r\pm\frac{z}{2}\right)e^{-ipz/\hbar}dz = 2\left(\frac{2}{\hbar}\right)^{1/2}e^{-\frac{r^2}{\hbar}}e^{-\frac{p^2}{\hbar}}(r\pm ip), \quad (18)$$

$$\int\phi_1\left(r-\frac{z}{2}\right)\phi_1\left(r+\frac{z}{2}\right)e^{-ipz/\hbar}dz = 2e^{-\frac{r^2}{\hbar}}e^{-\frac{p^2}{\hbar}}\left(\frac{2}{\hbar}(r^2+p^2)-1\right), \quad (19)$$

one can easily show that

$$g_{\lambda\lambda'}(x) = \frac{2^{N+1}}{\hbar}e^{-\frac{x^2}{\hbar}}\left(r_\lambda r_{\lambda'} + p_\lambda p_{\lambda'} - i(r_\lambda p_{\lambda'} - r_{\lambda'}p_\lambda) - \frac{\hbar}{2}\delta_{\lambda\lambda'}\right) \quad (20)$$

In addition, from Eq. (4),

$$\langle m_{\lambda'}|\hat{\rho}_m|m_\lambda\rangle = \rho_W^{\lambda\lambda'}(X) \quad (21)$$

Thus, the time variation of the physical observable becomes

$$\langle O(t)\rangle = \frac{1}{(2\pi\hbar)^N}\sum_{\lambda\lambda'}\int O_m(x,X,t)g_{\lambda\lambda'}(x)\rho_W^{\lambda\lambda'}(X)dXdx = \int O_m(x,X,t)\tilde{\rho}_m(x,X)dxdX \quad (22)$$

where we have defined $\tilde{\rho}_m$ as

$$\tilde{\rho}_m(x,X) = \frac{1}{(2\pi\hbar)^N}\sum_{\lambda\lambda'}g_{\lambda\lambda'}(x)\rho_W^{\lambda\lambda'}(X) \quad (23)$$

Therefore, to find the average evolution of any observable O in time, whose adiabatic representation is known as $O_W^{\lambda\lambda'}$, one first performs sampling of $x = (r, p)$ at time zero that can adequately represent the initial density matrix $\tilde{\rho}_m$, and integrates the equations of motion for the subsystem and bath variables. At a later time t, the new distribution in (r, p) is used to obtain $O_m(x, X, t)$ with the help of Eq. (4) as

$$O_m(x,X,t) = \frac{1}{2}\sum_{\lambda\lambda'}O_W^{\lambda\lambda'}(X)(r_\lambda r_{\lambda'} + p_\lambda p_{\lambda'} - i(r_\lambda p_{\lambda'} - r_{\lambda'}p_{\lambda'}) - \hbar\delta_{\lambda\lambda'}) \quad (24)$$

It is noted that the imaginary part of the above equation vanishes if $\hat{O}_W$ is Hermitian. In any case, this time dependent quantity is combined with the initial distribution $\tilde{\rho}_m$ to get the time dependent average $\langle O(t)\rangle$. For population and coherence dynamics, the appropriate operator for $\hat{O}_W$ is of course $|\lambda\rangle\langle\lambda'|$. For example, the population on site 1 is observed with $O_w^{\lambda\lambda'} = \delta_{\lambda,1}\delta_{\lambda',1}$.

The evolution of phase space variables is performed with the following Trotter decomposition scheme.[16] We split H_m as $H_m = H_1 + H_2$ with $H_1 = P^2/2M$ and $H_2 = V_e + h_m$, and the time evolution operator over Δt is decomposed as

$$e^{-i\hat{L}\Delta t} = e^{-i\hat{L}_1\Delta t/2}e^{-i\hat{L}_2\Delta t}e^{-i\hat{L}_1\Delta t/2} \quad (25)$$

with apparent definitions for $\hat{L}_1$ and $\hat{L}_2$. During the first $\Delta t/2$ step, R changes to $R + P\Delta t/2M$, while others are kept constant. The next task is to apply the middle operator $e^{-i\hat{L}_2\Delta t}$, to integrate the equations for positions and momenta with Eq. (9). Because h is Hermitian, it is diagonalizable and the differential equations of the subsystem variables can be solved exactly. Namely, with $\tilde{h} = D^{-1}hD$, dressed coordinates and momenta of the quantum subsystem are written as

$$\tilde{r} = D^{-1} r\,,$$
$$\tilde{p} = D^{-1} p\,, \tag{26}$$

and the differential equations based on these dressed terms are

$$\frac{d\tilde{r}_\lambda}{dt} = \frac{1}{\hbar}\varepsilon_\lambda(R)\tilde{p}_\lambda\,,$$
$$\frac{d\tilde{p}_\lambda}{dt} = -\frac{1}{\hbar}\varepsilon_\lambda(R)\tilde{r}_\lambda\,,$$
$$\frac{dR}{dt} = 0\,,$$
$$\frac{dP}{dt} = -\frac{\partial V_e}{\partial R} - \frac{1}{2\hbar}\sum_\lambda \frac{\partial \varepsilon_\lambda(R)}{\partial R}(\tilde{r}_\lambda^2 + p_\lambda^2 - \hbar) \tag{27}$$

As explained in the above, ε_λ is the λ-th eigenvalue of h or the adiabatic energy of the system. One may have a concern that the derivative of ε_λ may not be easily obtained as it is only calculated through numerical iterations in general. However, it is trivial to show that

$$\frac{\partial \varepsilon_\lambda}{\partial R} = D_{\mu\lambda}\frac{\partial h_{\mu\mu'}}{\partial R}D_{\mu'\lambda} \tag{28}$$

One can notice that the differential equations of the subsystem has been simplified due to the diagonal nature of $\tilde{h}$. With a super-matrix representation, they are

$$\frac{d}{dt}\begin{bmatrix}\tilde{r}_\lambda \\ \tilde{p}_\lambda\end{bmatrix} = \frac{1}{\hbar}\begin{bmatrix}0 & \varepsilon_\lambda(R) \\ -\varepsilon_\lambda(R) & 0\end{bmatrix}\begin{bmatrix}\tilde{r}_\lambda \\ \tilde{p}_\lambda\end{bmatrix} \tag{29}$$

and the solution is given as

$$\begin{bmatrix}\tilde{r}_\lambda(t+\Delta t) \\ \tilde{p}_\lambda(t+\Delta t)\end{bmatrix} = \begin{bmatrix}\cos(\varepsilon_\lambda/\hbar\Delta t) & \sin(\varepsilon_\lambda/\hbar\Delta t) \\ -\sin(\varepsilon_\lambda/\hbar\Delta t) & \cos(\varepsilon_\lambda/\hbar\Delta t)\end{bmatrix}\begin{bmatrix}\tilde{r}_\lambda(t) \\ \tilde{p}_\lambda(t)\end{bmatrix} \tag{30}$$

Because the transform matrix with the trigonometric functions is unitary, it is easy to see that $\tilde{r}(t)^2 + \tilde{p}(t)^2$ is time-invariant. Therefore, the integration for P is simplified as

$$P(t+\Delta t) = -\frac{\partial V_e}{\partial R}\Delta t - \frac{1}{2\hbar}\frac{\partial \varepsilon_\lambda(R)}{\partial R}\Delta t(\tilde{r}^2(t) + \tilde{p}^2(t) - \hbar) \tag{31}$$

Then, we perform the inverse transformation of Eq. (26) to the subsystem variables to get r and p, which completes the operation of the middle propagator in Eq. (25). This is followed by the final step of applying the leftmost operator in the Trotter decomposition, which is operationally equivalent to the propagation with the first $\Delta t/2$ step.

For a practical reason, one additional modification can be used during the time propagation. The transformation

$$\bar{h}_{\lambda\lambda'} = h_{\lambda\lambda'} - \alpha\delta_{\lambda\lambda'} \tag{32}$$

conserves the eigenvectors of h as the column vectors of D and changes the eigenvalues ε_i into $\varepsilon_i - \alpha$. If we use α = Tr(h)/N, the trace of $\bar{h}$ will of course be zero. Then,

$$\frac{d\tilde{r}_\lambda}{dt} = \frac{1}{\hbar}\bar{\varepsilon}_\lambda(R)\tilde{p}_\lambda + \frac{\alpha}{\hbar}\tilde{p}_\lambda\,,$$
$$\frac{d\tilde{p}_\lambda}{dt} = -\frac{1}{\hbar}\bar{\varepsilon}_\lambda(R)\tilde{r}_{\lambda'} - \frac{\alpha}{\hbar}\tilde{r}_\lambda\,,$$
$$\frac{dR}{dt} = 0\,,$$
$$\frac{dP}{dt} = -\frac{\partial V_e}{\partial R} - \frac{1}{2\hbar}\sum_\lambda\left(\frac{\partial \bar{\varepsilon}_\lambda(R)}{\partial R} + \frac{\partial \alpha}{\partial R}\right)(\tilde{r}_\lambda^2 + \tilde{p}_\lambda^2) + \frac{1}{2}\left(\frac{\partial \mathrm{Tr}(\bar{h})}{\partial R} + \frac{\partial \mathrm{Tr}(\alpha)}{\partial R}\right) \tag{33}$$

We can then ignore all terms involving α as an approximation. Even though this "traceless approach" is mathematically not equivalent because the trace changes in time in general and the results may become different as a result, this may stabilize the trajectory integrations. This can be easily understood when one considers the characteristics of the propagation equations for $\tilde{r}$ and $\tilde{p}$. Because their rates of change directly depend on the Hamiltonian components, not the derivatives of the Hamiltonian, they may vary in time very quickly when the trace of the h matrix is large. Trace removal at least minimizes this drawback, similarly to the variable changing scheme in the semiclassical treatment of the spin boson model.[17]

Model Hamiltonian of PC645. The model Hamiltonian used in this work for the PC645 light harvesting system is[10]

$$H_{\mathrm{total}} = H_{\mathrm{subsystem}} + H_{\mathrm{coupling}} + H_{\mathrm{bath}} \tag{34}$$

The subsystem Hamiltonian has the following term

$$H_{\mathrm{subsystem}} = \sum_{k=1}^{N}\sum_{k'=1}^{N}\{\varepsilon_k\delta_{kk'} + \Delta_{kk'}(1-\delta_{kk'})\}|k\rangle\langle k'|\,, \tag{35}$$

where N is the number of states (N = 8 in the case of PC645). The diagonal element ε_k is the k-th electronic site energy, and the off-diagonal element $\Delta_{kk'}$ is the electronic coupling between k-th and k'-th pigments. All the values of site energies and coupling strengths are shown in Table 1.

The coupling Hamiltonian has the following form

$$H_{\mathrm{coupling}} = \sum_{k=1}^{N}\left\{\sum_{l=1}^{n^{(k)}} c_l^{(k)}R_l^{(k)} + \sum_{j=1}^{N}\sum_{m=1}^{n^{(j)}}\frac{1}{2}(P_m^{(j)2} + \omega_m^{(j)2}R_m^{(j)2})\right\}|k\rangle\langle k| \tag{36}$$

The spectral density, $j(\omega)$, is the sum of two different Debye densities:

$$j(\omega) = 2\lambda_0\left[\frac{\omega\tau_1}{(\omega\tau_1)^2+1} + \frac{\omega\tau_2}{(\omega\tau_2)^2+1}\right] \tag{37}$$

with λ_0 = 130 cm^{-1}, which is actually the half of the reorganization energy. Of course, the spectral density has a close relationship with the system-bath coupling. The simulations were performed with τ_1 = 50 fs and τ_2 = 1.5 ps following Huo and Coker.[10]

The initial density matrix was assumed as $\rho_{\mathrm{total}}(0) = \rho_S(0)\rho_B(0)$. The subsystem part $\rho_S(0)$ reflects the initial condition of the pigment system. In this work, we have assumed that the initial excitation is located at the pigment DBVc with all other pigments remaining in the ground state. Thus, by designating DBVc with the pigment index k=1, $[\rho_s(0)]_{11}$=1

Table 1. Parameters of $H_{subsystem}$ for PC645 as adopted from refs. 3 and 7. Energies are in cm^{-1} unit. Because the matrix is symmetric, only its upper triangular components are shown

Bilin	DBVc	DBVd	MBVa	MBVb	PCBc158	PCBd158	PCBc82	PCBd82
DBVc	17034	319.4	–9.6	–43.9	20.3	25.3	–46.8	–20.0
DBVd		17116	43.9	7.7	30.5	29.0	21.5	48.0
MBVa			16050	4.3	–86.7	–2.9	–15.8	49.3
MBVb				16373	3.4	86.2	53.8	–14.7
PCBc158					15808	7.8	11.0	10.0
PCBd158						15889	29.0	–10.7
PCBc82							15566	48.0
PCBd82								15647

and all the other density matrix elements are zero. The phonon bath associated with the l-th site is assumed to follow the Gaussian distribution[8]

$$\rho_{W,e}^{(l)}(X) = \prod_k \frac{1}{2\pi} \frac{\beta\omega_k \tanh(\beta\hbar\omega_k/2)}{\beta\hbar\omega_k/2} \exp\left[-\frac{\tanh(\beta\hbar\omega_k/2)}{\hbar\omega_k/2} (P_k^2 + \omega_k R_k^2) \right] \tag{38}$$

by assuming that H_{bath} is composed of the classical harmonic oscillators with frequencies $\{\omega_k\}$.

The PBME trajectories were simulated by sampling 5000 independent trajectories with random (r_k, p_k) values obtained according to their appropriate Wigner distributions after considering Eq. (23). Because we can only use discrete representation $\tilde{\rho}_m(x,X) \rightarrow \{x_i\}$ with corresponding weights $\{w_i\}$ at any given X, the integration is replaced with a summation over the ensemble of $\{x_i\}$:

$$\langle O(t) \rangle = \sum_X \sum_i w_i O_m(x_i, X, t) \tag{39}$$

We have adopted a readily available routine for generating random numbers according to a Gaussian distribution $P(r_\lambda, p_\lambda) = \exp[-(r_\lambda^2 + p_\lambda^2)/\hbar]/\pi\hbar$. Thus the weights are given as

$$w_i = 2 \sum_{\lambda\lambda'} \left[\frac{1}{\hbar} \left(r_\lambda r_{\lambda'} + p_\lambda p_{\lambda'} - i(r_\lambda p_{\lambda'} - r_{\lambda'} p_\lambda) - \frac{1}{2}\delta_{\lambda\lambda'} \right) \right] \rho_W^{\lambda'\lambda}(X) \tag{40}$$

The population dynamics and the development of the coherence were monitored by treating the distributions of these mapping variables in time with Eq. (39).

Results and Discussion

Figure 1 shows the dynamics for the full eight site model of PC645 for both the diagonal and off-diagonal elements of the density matrix. The simulations began with the initial excitation of DBVc pigment at $T = 294$ K. Figure 1(a) indeed shows very strong coherent beating between DBVc and DBVd which are coupled to each other up to 500 fs time scale. Populations of the other pigments show very slowly increasing behavior. Among these remaining six pigments, the population of MBVb grows peculiarly faster. This is likely because MBVb is relatively strongly coupled to DBVc and because the site energies of MBVb and DBVc are not too different, and it shows that efficient energy transfer requires both energy matching and a large coupling. Figure 1(b) also shows that initially only DBV dimer exhibits a very strong coherence. This coherence quenches after about 200 fs. With the adopted simple model Hamiltonian, however,

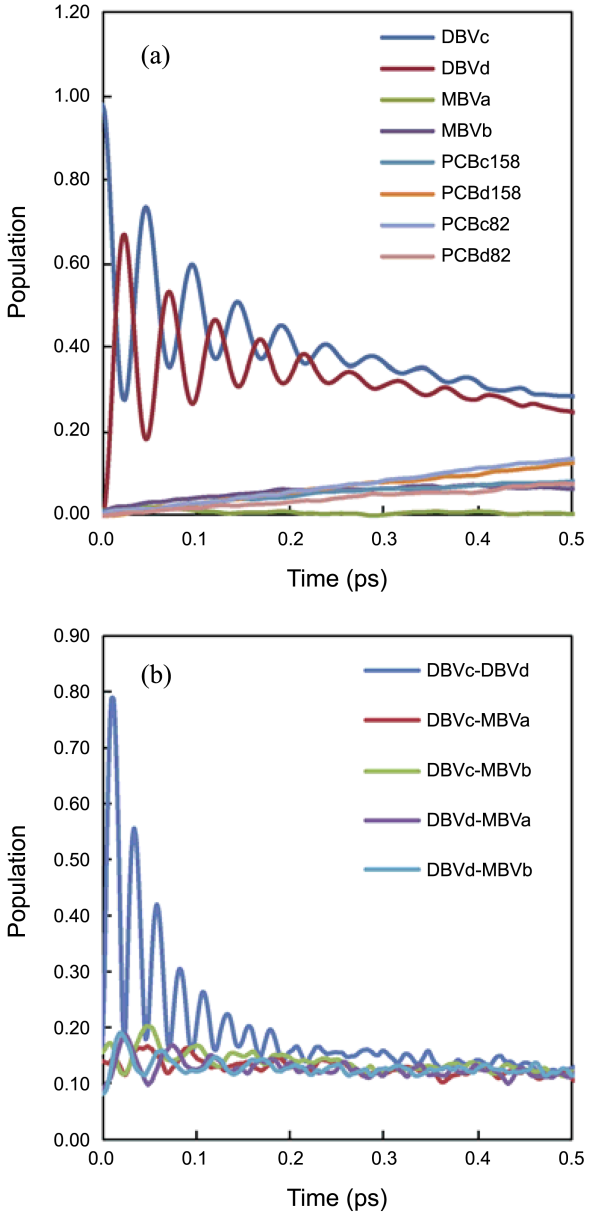

Figure 1. Energy transfer dynamics in PC645 after the initial excitation of DBVc at 294 K. (a) Population dynamics represented by the diagonal elements of the density matrix. (b) Time variations in concurrences represented by the off-diagonal elements.

it is not clear whether this decoherence is a pure dephasing effect or ensemble dephasing. Such a distinction will likely require all-atom type model where the differences in different molecular complexes can be properly represented. In any case, all these observations are in excellent agreement with the ILDM results reported by Huo and Coker,[10] which shows the reliability PBME at least in the short time domain (~1 ps).

When the simulations were extended beyond 1 ps, the results start to deviate from what we would expect from ILDM. Figure 2(a) shows the same dynamics of PC645 up to 10 ps. One important feature to notice from this figure in relation with Table 1 is the fact that the populations among chromophores are at least in the right order in terms of their energies. Namely, a site with higher energy has lower population. However, we see that their relative proportions do not follow the Boltzmann distribution. Mathematically, there is not even a guarantee that the populations will always be positive, and indeed, the figure shows some negative populations in the long time limit. This artifact is caused by the fact that the third term in Eq. (7) is ignored. The ignored term is known to correspond to one quarter of the dissipation.[8] Because the dissipation effect is not fully incorporated, the quantum subsystem will likely heat up. From Figure 2(a), however, we conclude that the quantum subsystem does not actually exhibit infinite temperature behavior with equal populations on all degrees of freedom as previously expected.[9] This is of course because a portion of the dissipation effect is still remaining in the formalism.

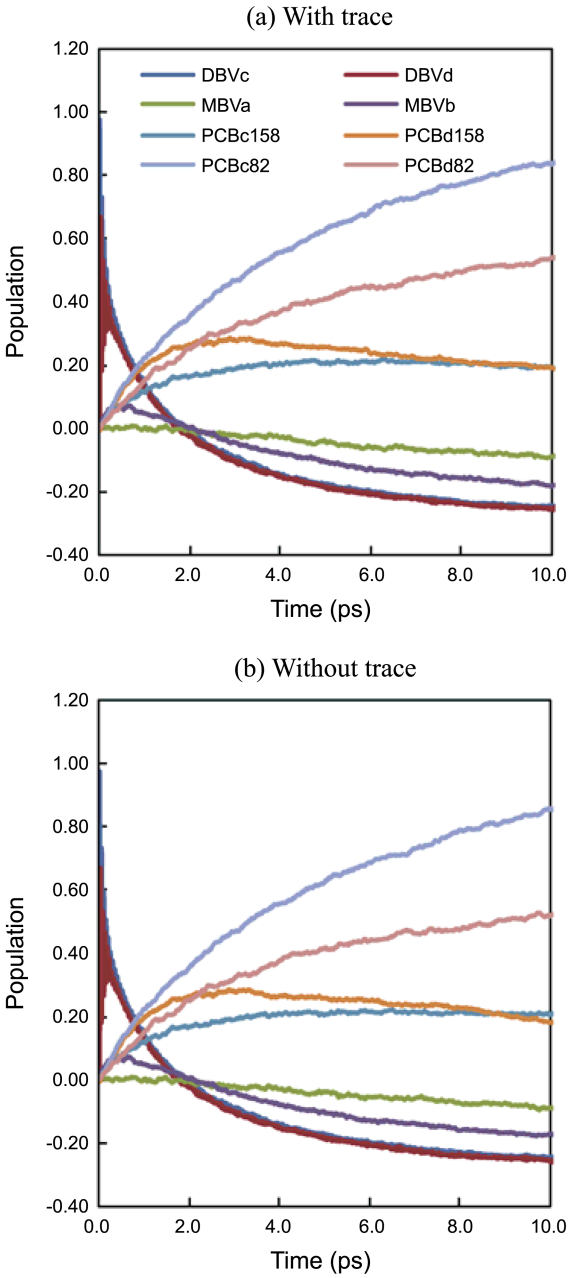

Figure 2. PBME Population dynamics in the long time regime obtained (a) with full subsystem Hamiltonian h_m and (b) with trace-eliminated Hamiltonian $\bar{h}_m$. Initial conditions are the same as in Fig. 1.

In addition, the issue of incorrect population is not eliminated even if we adopt the traceless model. In fact, as is shown in Figure 2(b), the traceless model generates qualitatively the same results compared to the dynamics with the trace. We expect that when there are excessive fluctuations in the energy, the traceless model may behave better as it will avoid the stiffness in Eq. (27) for integrating the quantum degrees of freedom (Eq. (26)). In any case, for future applications of PBME toward long time dynamics, a modification will be required to realize the correct equilibrium property.

The Debye or Ohmic spectral densities, which are often adopted in simplified models of open quantum systems, usually peak in the low frequency region and decay smoothly to zero in the high frequency. (See Fig. 3(a) showing the sum of two different Debye spectral densities.) When the spectral density is simulated with conventional classical MD simulations, however, large peaks are often observed in the high

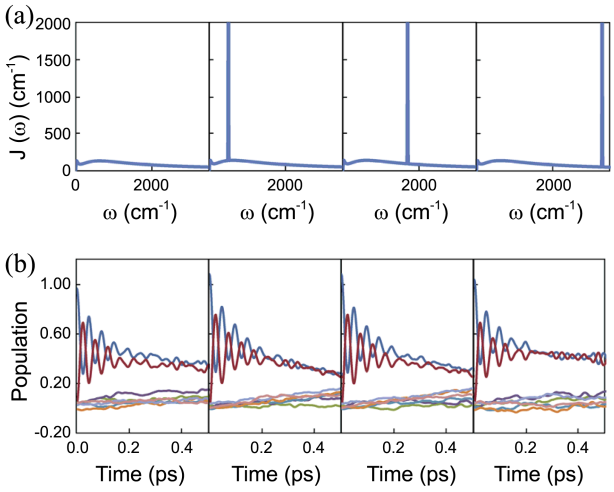

Figure 3. Effects of spurious high frequency modes in the spectral density. (a) Adopted spectral densities. The leftmost one is sum of two Debye functions with 50 fs and 1.5 ps relaxation times. The other three include additional Gaussian peaks centered at 500, 1700, 3300 cm^{-1} from left to right. (b) Population evolutions corresponding to the above spectral densities. See Fig. 1 for the coloring scheme of chromophore identifications.

frequency region where the normal Debye or Ohmic densities are usually very small.[18,19] Such peaks are of course artifacts of classical simulations: when a vibrational mode is described classically with many other bath modes, it will only have average energy that corresponds to the classical equipartition (k_BT). For a high frequency vibration, this energy is much smaller than the zero point energy $\hbar\omega/2$. Therefore, the phase space distribution sampled by a classical canonical ensemble for such vibration will be much narrower than the supposedly accurate Wigner distribution obtained based on quantum mechanical information. We speculate that this discrepancy is the cause of the spurious peaks in the spectral density. Even though it is not clear at this stage how to eliminate this artifact[18,19] from classical trajectory based approaches, we can at least test how large its effect is on the coherence dynamics of the energy transfer process.

Thus, we have mimicked this situation with additional sharp Gaussian shaped functions to the adopted spectral density:

$$f(\omega) = ae^{-(\omega-\omega_0)^2/2b^2} \quad (41)$$

with a = 0.8 eV and b = 30.0 cm^{-1}. The results are presented with Fig. 3 with the adopted spectral densities (top panels) and the corresponding population dynamics (bottom panels). For reference, the spectral density and the dynamics with no additional Gaussian peaks are shown in the leftmost panels. The remaining panels show the results obtained with ω_0 = 500 cm^{-1}, 1700 cm^{-1}, and 3300 cm^{-1} (from left to right). The reorganization energies with the adopted spectral densities change from λ = 260.0 cm^{-1} without a Gaussian peak to 274.9, 264.0, and 261.8 cm^{-1} for the three cases. In all three cases, one can clearly see that the population dynamics and the aspect of coherence/decoherence are only slightly affected. In a sense, this is not surprising as the energy transfer dynamics is mostly affected by the change in the reorganization energy. As can be shown with the changes in λ, spurious peaks in the high frequency region has limited effect on the reorganization energy. Even when the peak was placed in a relatively low frequency region (500 cm^{-1}), the reorganization energy was affected by ~5% and the energy transfer dynamics was only slightly modified. Therefore, we can infer that the artifact caused by such spurious peaks in high frequency part of the spectral density will be only marginal. Of course, when there are too many such peaks, the reorganization energy will be severely affected with the loss of coherence much earlier than normal. In this case, we have at least generated the peak shape (a and b) based on the spectral density reported by Olbrich et al on the FMO system,[19] and we do not expect the situation will be significantly different in other cases.

Conclusion

With an eight-site model of PC645 protein complex at physiological temperature, we have applied the PBME method to show its performance in describing energy transfer dynamics and the related coherence effect. When the DBVc chromophore was initially excited, the strongly coupled DBV pair showed strong coherent beating up to 500 fs and gradually, the excitation energy in the dimer migrated to other pigments. The population and coherence dynamics were in good accord with more reliable ILDM results. When the simulations were continued over a picosecond, PBME results deteriorated into non-Boltzmann distribution, confirming that the approximate nature of PBME renders it inappropriate for studying long time behaviors. Nevertheless, the dynamics from PBME within a picosecond is quite reliable especially in reproducing the correct oscillations in the population transfer. The result of adding artificial peaks to the spectral density functions did not make any noticeable changes to the energy transfer dynamics. This is encouraging for future studies of all-atom style PBME dynamics, where the classical representations of molecular vibrations will likely induce spurious high frequency peaks in the spectral density.

Acknowledgments. This work was supported by the POSTECH Basic Science Research Institute Grant. It was also supported by WCU Program (Grant No. R32-2008-000-10180-0) and Basic Science Research Program (Grant Nos. 2009-0067085) through the National Research Foundation of Korea (NRF) funded by the Korean Ministry of Education, Science, and Technology. The supercomputer time from Korea Institute of Science and Technology Information (KISTI) under Grant No. KSC-2011-C3-12 is also gratefully acknowledged.

References and Notes

1. Lee, H.; Cheng, Y.-C.; Fleming, G. R. *Science* **2007**, *316*, 1462.
2. Engel, G. S.; Calhoun, T. R.; Read, E. L.; Ahn, T.-K.; Mancal, T.; Cheng, Y.-C.; Blankenship, R. E.; Fleming, G. R. *Nature* **2007**, *446*, 782.
3. Collini, E.; Wong, C. Y.; Wilk, K. E.; Curmi, P. M. G.; Brumer, P.; Scholes, G. D. *Nature* **2010**, *463*, 644.
4. Panitchayangkoona, G.; Hayes, D.; Fransted, K. A.; Caram, J. R.; Harel, E.; Wen, J.; Blankenship, R. E.; Engel, G. S. *Proc. Natl. Acad. Sci. U.S.A.* **2010**, *107*, 12766.
5. van der Weij-De Wit, C. D.; Doust, A. B.; van Stokkum, I. H. M.; Dekker, J. P.; Wilk, K. E.; Curmi, P. M. G.; van Grondelle, R. *Biophys. J.* **2008**, *94*, 2423.
6. Wedemayer, G. J.; Kidd, D. G.; Wemmer, D. E.; Glazer, A. N. *J. Biol. Chem.* **1992**, *267*, 7315.
7. Mirkovic, T.; Doust, A. B.; Kim, J.; Wilk, K. E.; Curutchet, C.; Mennucci, B.; Cammi, R.; Curmi, P. M. G.; Scholes, G. D. *Photochem. Photobio. Sci.* **2007**, *6*, 964.
8. Kim, H.; Nassimi, A.; Kapral, R. *J. Chem. Phys.* **2008**, *129*, 084102.
9. Kelly, A.; Rhee, Y. M. *J. Phys. Chem. Lett.* **2011**, *2*, 808.
10. Huo, P.; Coker, D. F. *J. Phys. Chem. Lett.* **2011**, *2*, 825.
11. Chandler, D. *Introduction to Modern Statistical Mechanics*. Oxford University Press, Inc.: New York, 1987.
12. Nassimi, A.; Bonella, S.; Kapral, R. *J. Chem. Phys.* **2010**, *133*, 134115.
13. Thoss, M. *Phys. Rev. A* **1999**, *59*, 64.
14. Kapral, R.; Ciccotti, G. *J. Chem. Phys.* **1999**, *110*, 8919.
15. Kapral, R. *Annu. Rev. Phys. Chem.* **2006**, *57*, 129.
16. Nassimi, A. A study of quantum-classical dynamics in the mapping

basis. Ph.D. Thesis, University of Toronto, 2011.
17. Wang, H.; Song, X.; Chandler, D.; Miller, W. H. *J. Chem. Phys.* **1999**, *110*, 4828.
18. Shim, S.; Rebentrost, P.; Valleau, S.; Aspuru-Gusik, A. *Biophys. J.* **2012**, *102*, 649.
19. Olbrich, C.; Strumpefer, J.; Schulten, K.; Kleinekathöfer, U. *J. Phys. Chem. Lett.* **2011**, *2*, 1771.